A Chemoproteomic Strategy for Direct and Proteome-wide Covalent Inhibitor Target-site Identification

Christopher M. Browne [1,2], Baishan Jiang [1,2], Scott B. Ficarro [1,2,3], Zainab M. Doctor [1,2], Jared L. Johnson [4], Joseph D. Card [1,3], Sindhu Carmen Sivakumaren [1,2], William M. Alexander [1,3], Tomer M. Yaron [4], Charles J. Murphy [4], Nicholas P. Kwiatkowski [1,2,5], Tinghu Zhang [1,2], Lewis C. Cantley [4], Nathanael S. Gray [1,2,†], Jarrod A. Marto [1,3,6,†].

[1] Department of Cancer Biology, Dana–Farber Cancer Institute, Boston, Massachusetts, USA,

[2] Department of Biological Chemistry and Molecular Pharmacology, Harvard Medical School, Boston, Massachusetts, USA,

[3] Blais Proteomics Center, Dana-Farber Cancer Institute,

[4] Meyer Cancer Center, Weill Cornell Medicine and New York Presbyterian Hospital, New York, NY, USA,

[5] Whitehead Institute for Biomedical Research, Cambridge, Massachusetts, USA,

[6] Department of Pathology, Brigham and Women's Hospital, Harvard Medical School

[†] To whom correspondence should be addressed:

Jarrod A. Marto (jarrod_marto@dfci.harvard.edu)

Nathanael S. Gray (nathanael_gray@dfci.harvard.edu)

Department of Cancer Biology, Dana-Farber Cancer Institute, 360 Longwood Avenue, LC-2208, Boston, MA, 02215, USA.

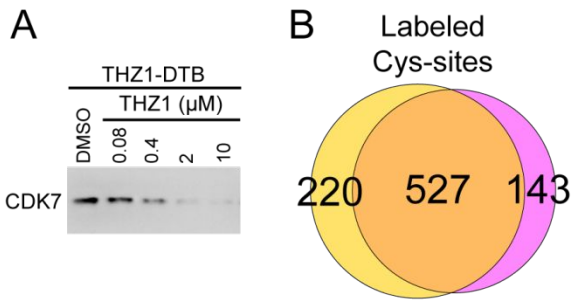

Figure S1

Supplementary Figure S1. (A) HeLa S3 lysates were treated in a competition-format with increasing concentrations of THZ1 followed by co-treatment with THZ1-DTB, streptavidin pulldown and immunoblot for CDK7. (B) Venn diagram illustrating the overlap of THZ1-DTB-modified cysteine residues identified across replicate CITe-Id experiments.

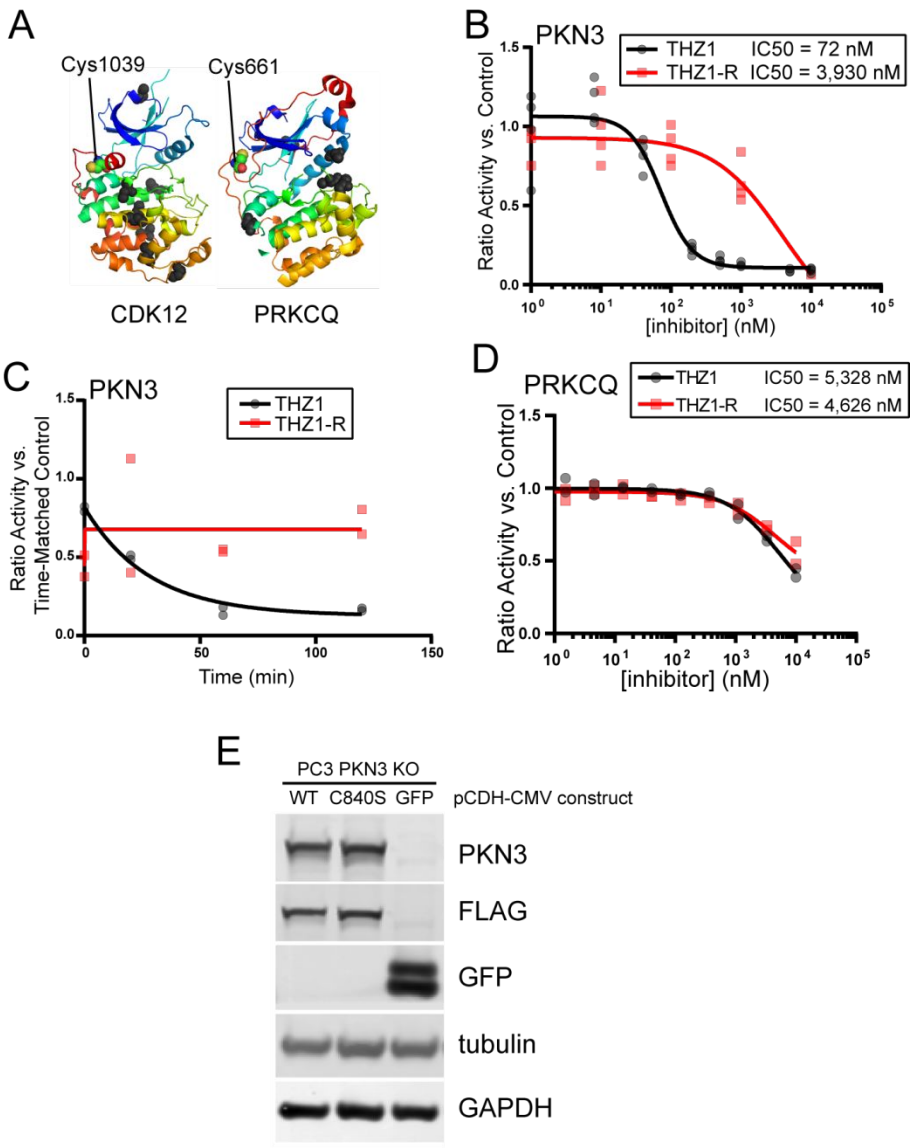

Figure S2

Supplementary Figure S2. (A) Structures of CDK12 and PRKCQ facing kinase active sites with cysteine labeling sites of THZ1-DTB highlighted as colored spheres. All other unlabeled cysteine residues are displayed as black spheres. (CDK12: PDB 4NST [1], PRKCQ: PDB 2JED). (B) *In Vitro* kinase assay for PKN3 inhibition. (C) *In Vitro* kinase assays performed as a time course for PKN3 inhibition. All time-points compared to time-matched DMSO control. (D) *In Vitro* kinase assays for inhibition of PRKCQ by THZ1 and THZ1-R. (E) Immunoblot of cell lysates from PC3 cells with CRISPR-CAS9 mediated PKN3 deletion expressing several FLAG-HA-tagged PKN3 rescue constructs.

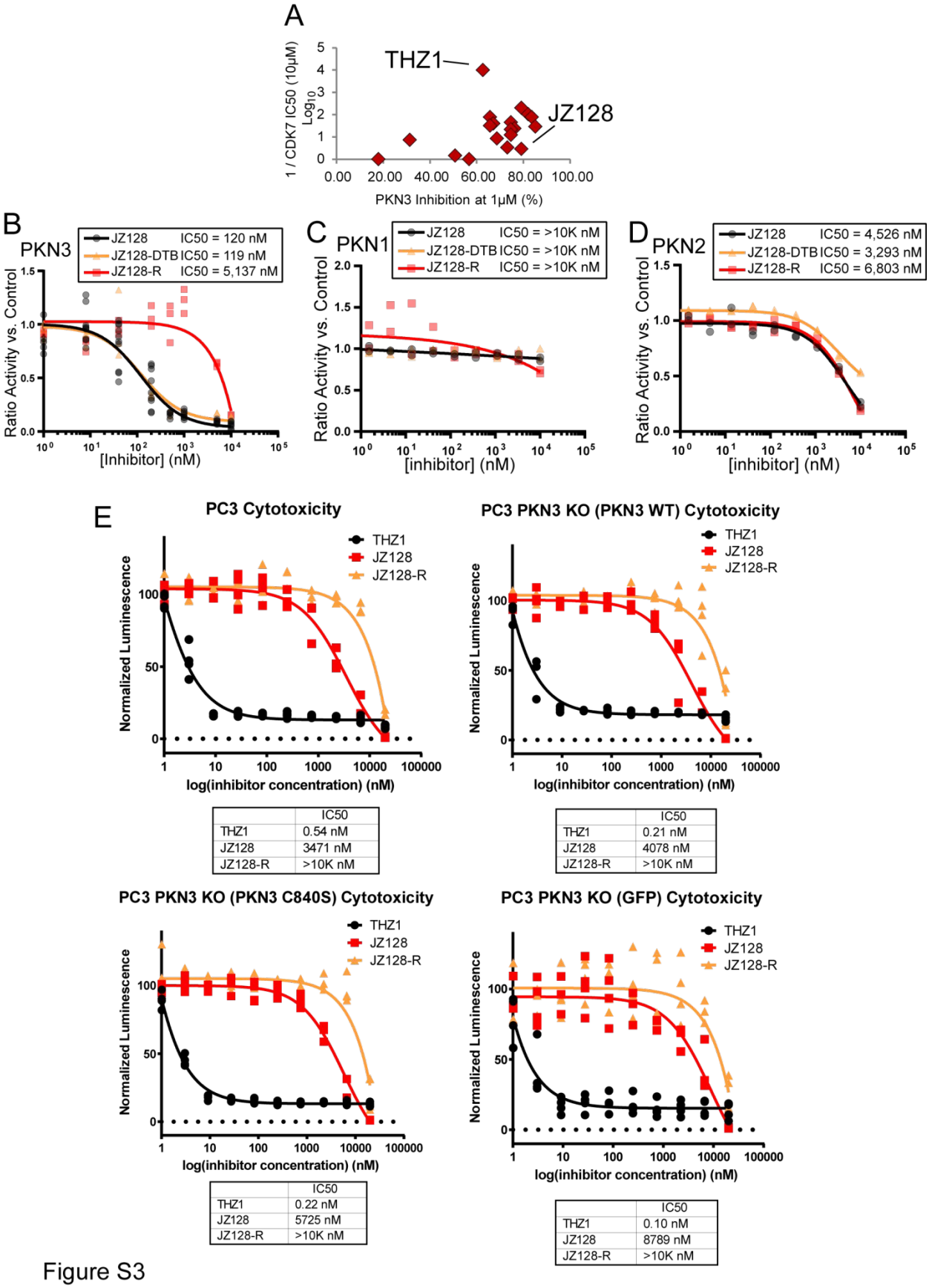
A
THZ1
JZ128
1 / CDK7 IC50 (10μM) Log10
PKN3 Inhibition at 1μM (%)
B
PKN3
JZ128 IC50 = 120 nM
JZ128-DTB IC50 = 119 nM
JZ128-R IC50 = 5,137 nM
Ratio Activity vs. Control
[Inhibitor] (nM)
C
PKN1
JZ128 IC50 = >10K nM
JZ128-DTB IC50 = >10K nM
JZ128-R IC50 = >10K nM
Ratio Activity vs. Control
[inhibitor] (nM)
D
PKN2
JZ128 IC50 = 4,526 nM
JZ128-DTB IC50 = 3,293 nM
JZ128-R IC50 = 6,803 nM
Ratio Activity vs. Control
[inhibitor] (nM)
E
PC3 Cytotoxicity
THZ1
JZ128
JZ128-R
Normalized Luminescence
log(inhibitor concentration) (nM)
IC50
THZ1 0.54 nM
JZ128 3471 nM
JZ128-R >10K nM
PC3 PKN3 KO (PKN3 WT) Cytotoxicity
THZ1
JZ128
JZ128-R
Normalized Luminescence
log(inhibitor concentration) (nM)
IC50
THZ1 0.21 nM
JZ128 4078 nM
JZ128-R >10K nM
PC3 PKN3 KO (PKN3 C840S) Cytotoxicity
THZ1
JZ128
JZ128-R
Normalized Luminescence
log(inhibitor concentration) (nM)
IC50
THZ1 0.22 nM
JZ128 5725 nM
JZ128-R >10K nM
PC3 PKN3 KO (GFP) Cytotoxicity
THZ1
JZ128
JZ128-R
Normalized Luminescence
log(inhibitor concentration) (nM)
IC50
THZ1 0.10 nM
JZ128 8789 nM
JZ128-R >10K nM

Figure S3

Supplementary Figure S3. (A) Graph comparing CDK7 activity to PKN3 activity of screened THZ1 analogs. Vertical axis shows the $\log_{10}$ inverse of the IC50 of CDK7 inhibition, horizontal axis is the % inhibition of PKN3 for each compound at 1μM concentration. (B-D) *In vitro* kinase assays for PKN3, PKN1, and PKN2 inhibition respectively. (E) Results of CellTiter-Glo® luminescent cell viability assays for PC3 rescue strains used in this study.

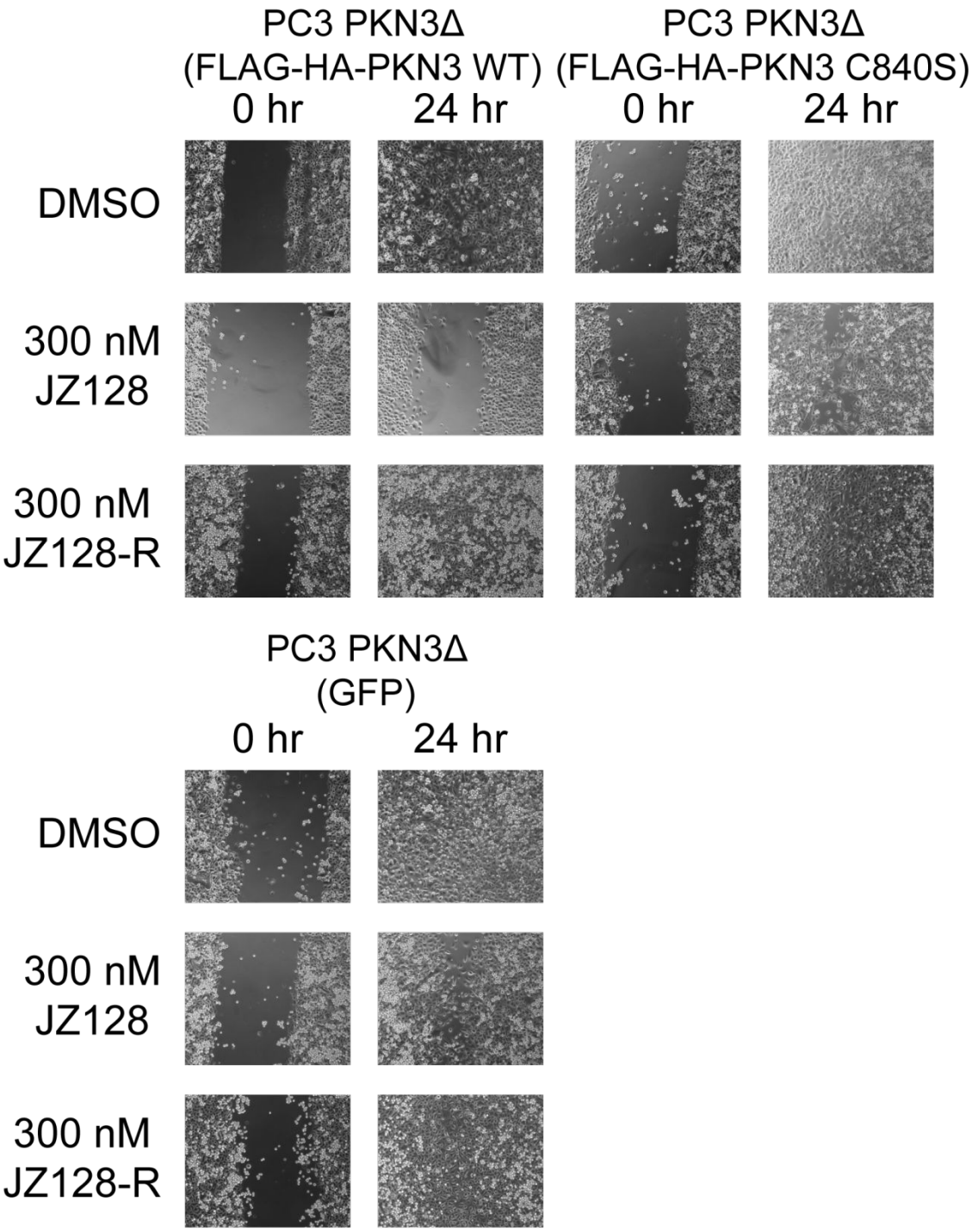

Figure S4

Supplementary Figure S4. Representative images of PC3 cell wound healing assays taken 0 h or 24 h after wounding.

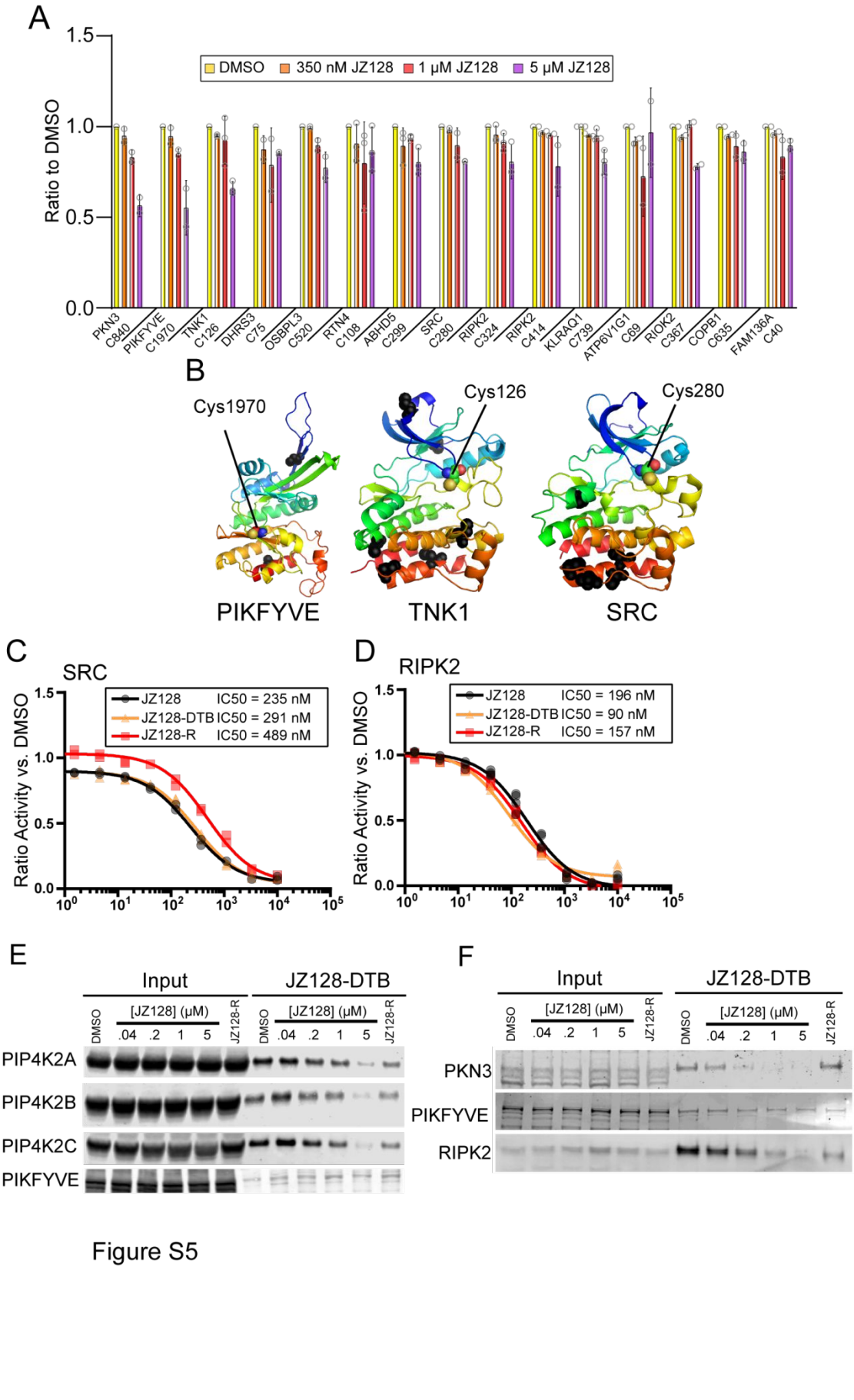
A
DMSO
350 nM JZ128
1 μM JZ128
5 μM JZ128
Ratio to DMSO
PKN3 C840
PIKFYVE C1970
TNK1 C126
DHRS3 C75
OSBPL3 C520
RTN4 C108
ABHD5 C299
SRC C280
RIPK2 C324
RIPK2 C414
KLRAQ1 C739
ATP6V1G1 C69
RIOK2 C367
COPB1 C635
FAM136A C40
B
Cys1970
Cys126
Cys280
PIKFYVE
TNK1
SRC
C
SRC
JZ128 IC50 = 235 nM
JZ128-DTB IC50 = 291 nM
JZ128-R IC50 = 489 nM
Ratio Activity vs. DMSO
D
RIPK2
JZ128 IC50 = 196 nM
JZ128-DTB IC50 = 90 nM
JZ128-R IC50 = 157 nM
Ratio Activity vs. DMSO
E
Input
JZ128-DTB
DMSO
[JZ128] (μM)
.04 .2 1 5
JZ128-R
PIP4K2A
PIP4K2B
PIP4K2C
PIKFYVE
F
Input
JZ128-DTB
PKN3
PIKFYVE
RIPK2

Figure S5

Supplemental Figure S5. (A) Replicate CITe-Id results for JZ128 and JZ128-DTB in PC3 lysates. Cysteine residues bound by JZ128-DTB in a concentration-dependent manner as indicated by a dose-response exceeding two standard deviations relative to the median value of all 686 reproducibly labeled cysteine residues. (B) Structures of PIKFYVE, TNK1, and SRC facing kinase active sites with cysteine labeling sites of JZ128-DTB highlighted as colored spheres. All other unlabeled cysteine residues are displayed as black spheres. (PIKFYVE: Swiss-Model Q9Y1I7, TNK1: Swiss-Model Q13470, SRC: PDB 1FMK [2]). (C,D) *In Vitro* kinase assays for SRC and RIPK2 inhibition. (E) Live HEK 293T cell treatments with JZ128 or JZ128-R. Lysates treated with JZ128-DTB, followed by streptavidin pulldown and immunoblotting against PIP4K2A-C homologs or PIKFYVE. (F) Live PC3 cell treatments with JZ128 or JZ128-R. Lysates treated with JZ128-DTB, followed by streptavidin pulldown and immunoblotting against PKN3, PIKFYVE, or RIPK2.

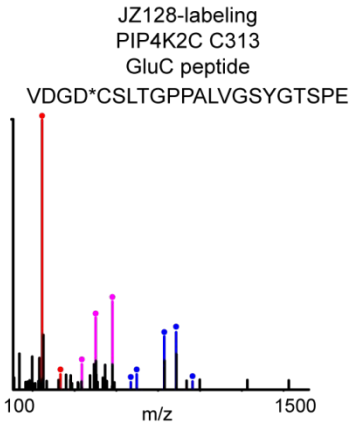

Figure S6

Supplemental Figure S6. MS2 spectra of JZ128-labeled, GluC digested PIP4K2C peptide containing Cys-313. Red: y ions, blue: b ions, pink: JZ128 specific fragment ions.

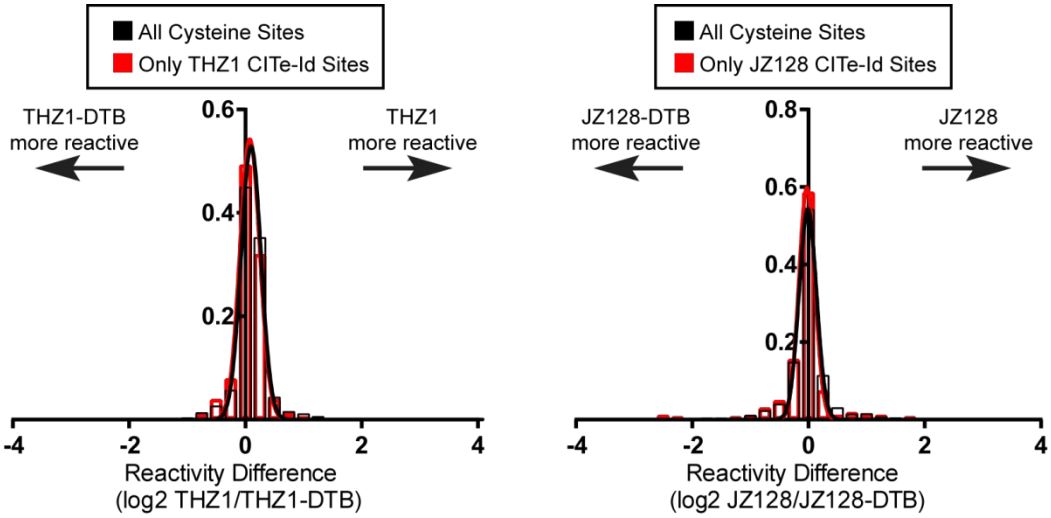

Figure S7

Supplementary Figure S7. Comparison of untagged and desthiobiotin-tagged compound reactivity. Shown are overlaid density histograms of the reactivity between the untagged and tagged compounds used in this study for all cysteine sites detected (black) and only sites also found to be covalently modified in the compounds' respective CITe-Id experiments (red). Both the bins and a

nonlinear regression for the data are included. Arrows indicate direction of higher reactivity for each compound. THZ1/THZ1-DTB comparison: all sites N = 1,177, CITe-Id sites N = 75; JZ128/JZ128-DTB comparison: all sites N = 854, CITe-Id sites N = 160. See Supplementary Table S4 for details.

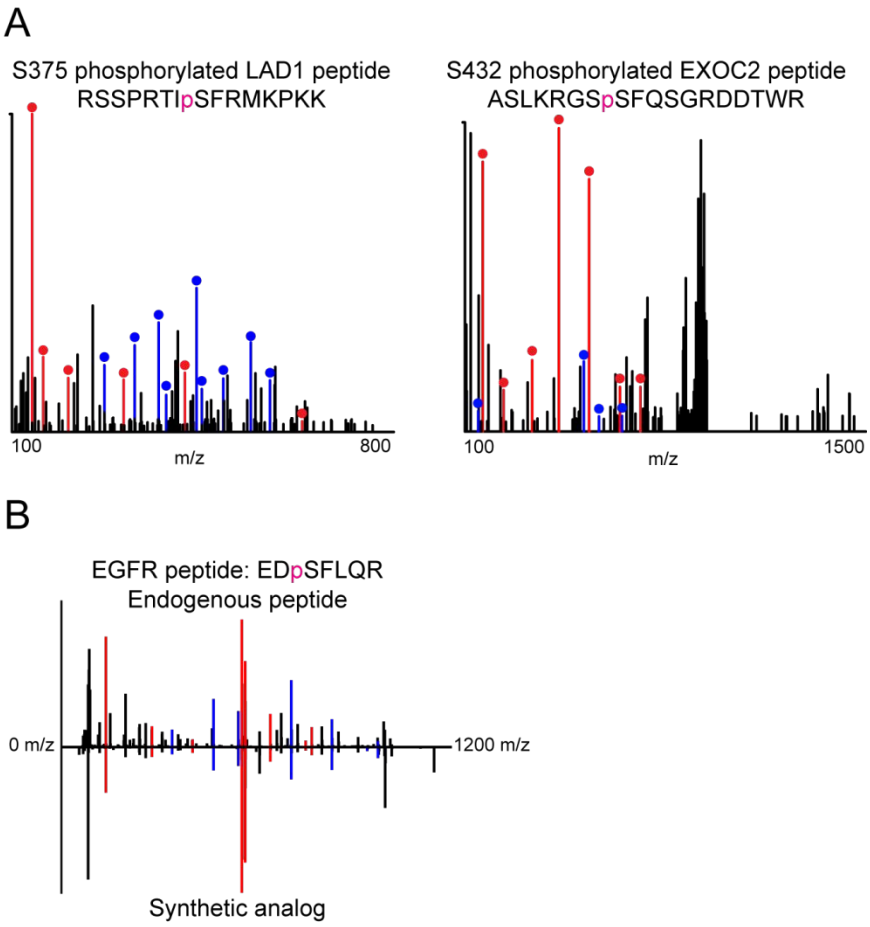

Figure S8

Supplemental Figure S8. Peptide sequence and phosphosite validation. (A) MS/MS spectra for the LAD1 S375 and EXOC2 S432 peptides phosphorylated *in vitro* by PKN3. y-type ions are colored red and b-type ions are colored blue. (B) MS/MS spectra for EGFR phosphopeptide observed in phosphoproteomic experiment (top) and the synthetic peptide analog (bottom). y-type ions are colored red and b-type ions are colored blue. Pink lower case 'p' indicates phosphorylation on the subsequent serine residue.

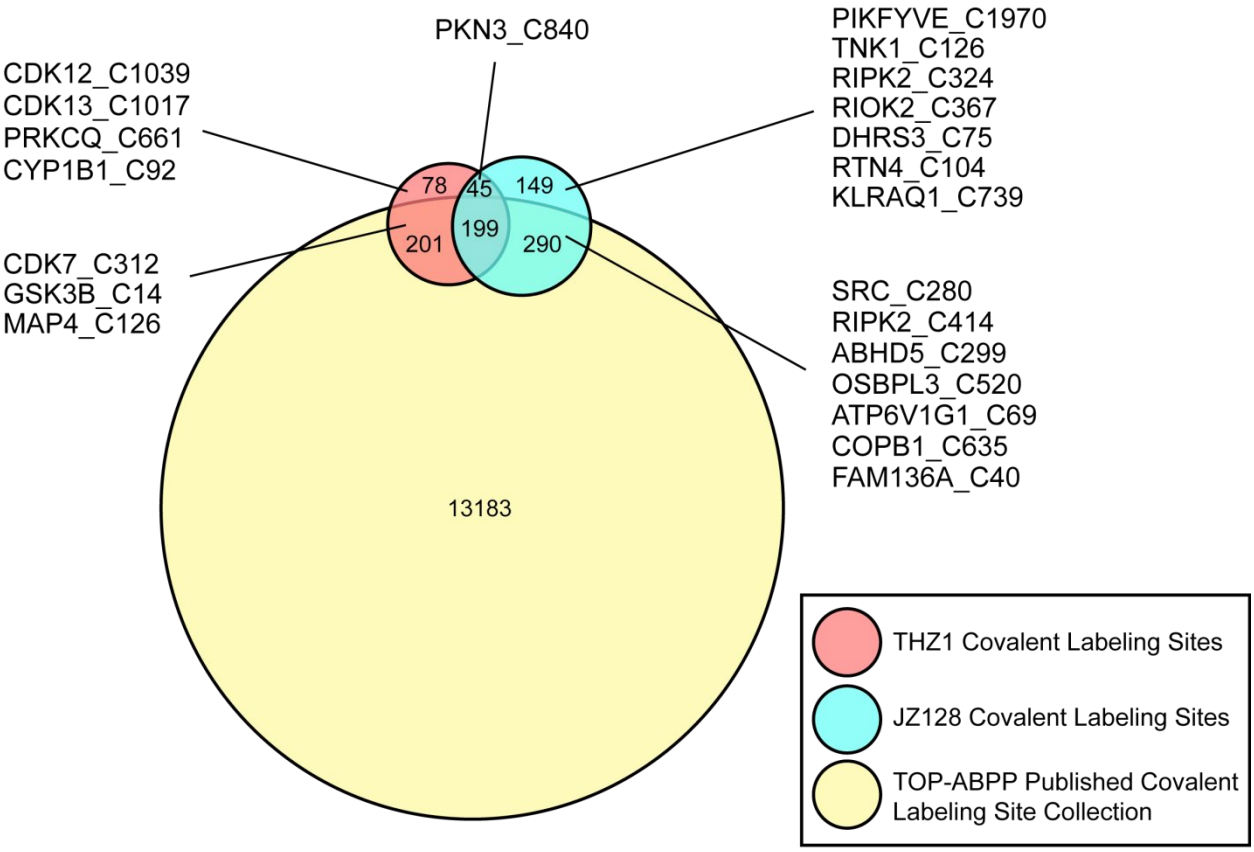

Figure S9

Supplementary Figure S9. Venn Diagram of reported cysteine labeling sites for THZ1, JZ128, and 8 seminal TOP-ABPP site-level publications [3-10]. Data represents the union of reported cysteine labeling sites. The 22 dose-dependent targets of THZ1 and JZ128 identified by CITe-Id are listed individually, along with the modified cysteine residue. Twelve of these 22 sites are unique to CITe-Id.

Supplementary Table S1. Fragment Ions Characteristic of THZ1-DTB and JZ128-DTB. Shown are names, m/z values, and chemical structures of fragment ions commonly seen in MS/MS spectra of peptides labeled with THZ1-DTB or JZ128-DTB. MGF files were pre-processed as described in [11] to account for these compound-specific fragment ions prior to database search.

Supplementary Table S2. CITe-Id Results. Each tab includes the genes and cysteine sites modified by each desthiobiotin-tagged inhibitor analog along with individual ratios for biological replicates. Labeled residue number corresponds to the first gene shown when a non-gene-unique peptide was identified. Peptide sequences and peptide-spectra matches (PSM) for each site are also included. Combined ratios were the average of biologic replicate ratios. Sample standard deviation of all biologic replicate ratios is also shown.

Supplementary Table S3.KiNativ Results. Kinase proteins and their percent inhibition by JZ128. Treatments were performed on live PC3 cells using 1 μM JZ128 for 3h.

Supplementary Table S4. Compound Reactivity Comparisons. Genes, cysteine sites, peptides, and untagged-/tagged-compound reactivity differences are displayed. The table also denotes if a cysteine site was detected as inhibitor-modified in its respective CITe-Id experiment.

Supplementary Table S5. Phosphoproteomics Results. Shown are genes and protein relative phosphorylation sites. For each phosphorylation site, the 14 residues surrounding it are shown for the purposes of phosphorylation motif scoring. For cases of multiply phosphorylated peptides, each phosphosite was given its own entry and surrounding sequence for motif scoring, all other information for the peptide was kept the same for each site.

Supplementary Table S6. PKN3 Phospho Motif Densitometry Inputs. Values were generated from two replicate PKN3 phospho motif arrays and used for scoring potential PKN3 substrate sites.

1 Bosken, C. A. *et al.* The structure and substrate specificity of human Cdk12/Cyclin K. *Nat Commun* **5**, 3505, doi:10.1038/ncomms4505 (2014).

2 Xu, W., Harrison, S. C. & Eck, M. J. Three-dimensional structure of the tyrosine kinase c-Src. *Nature* **385**, 595-602, doi:10.1038/385595a0 (1997).

3 Abo, M. & Weerapana, E. A Caged Electrophilic Probe for Global Analysis of Cysteine Reactivity in Living Cells. *J Am Chem Soc* **137**, 7087-7090, doi:10.1021/jacs.5b04350 (2015).

4 Backus, K. M. *et al.* Proteome-wide covalent ligand discovery in native biological systems. *Nature* **534**, 570-574, doi:10.1038/nature18002 (2016).

5 Bak, D. W., Pizzagalli, M. D. & Weerapana, E. Identifying Functional Cysteine Residues in the Mitochondria. *ACS chemical biology* **12**, 947-957, doi:10.1021/acschembio.6b01074 (2017).

6 Deng, X. *et al.* Proteome-wide quantification and characterization of oxidation-sensitive cysteines in pathogenic bacteria. *Cell Host Microbe* **13**, 358-370, doi:10.1016/j.chom.2013.02.004 (2013).

7 Quinti, L. *et al.* KEAP1-modifying small molecule reveals muted NRF2 signaling responses in neural stem cells from Huntington's disease patients. *Proceedings of the National Academy of Sciences of the United States of America* **114**, E4676-E4685, doi:10.1073/pnas.1614943114 (2017).

8 Weerapana, E. *et al.* Quantitative reactivity profiling predicts functional cysteines in proteomes. *Nature* **468**, 790-795, doi:10.1038/nature09472 (2010).

9 Bar-Peled, L. *et al.* Chemical Proteomics Identifies Druggable Vulnerabilities in a Genetically Defined Cancer. *Cell* **171**, 696-709 e623, doi:10.1016/j.cell.2017.08.051 (2017).

10 Blewett, M. M. *et al.* Chemical proteomic map of dimethyl fumarate-sensitive cysteines in primary human T cells. *Sci Signal* **9**, rs10, doi:10.1126/scisignal.aaf7694 (2016).

11 Ficarro SB, B. C., Card JD, Alexander WM, Zhang T, Park E, McNally R, Dhe-Paganon S, et al. Leveraging gas-phase fragmentation pathways for improved identification and selective detection of targets modified by covalent probes. *Anal Chem.* **88**, 12248-12254 (2016).